Supplemental Figure 1

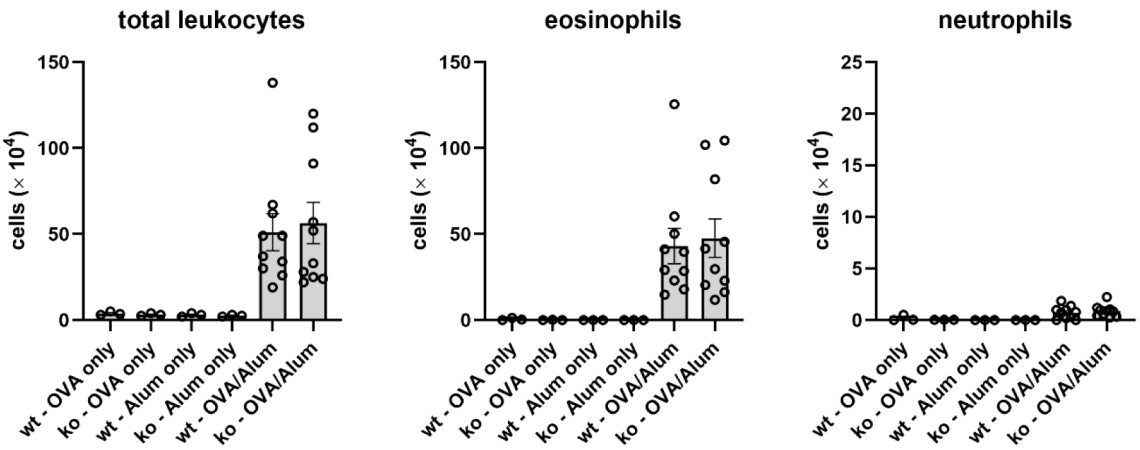

Supplemental Figure 1. *P2ry14* is dispensable for airway inflammation in the alum/OVA model of asthma. Shown are cell numbers for the indicated cell types 48 h post-OVA challenge in mice previously sensitized by i.p. injections of alum/OVA.

Supplemental Figure 2

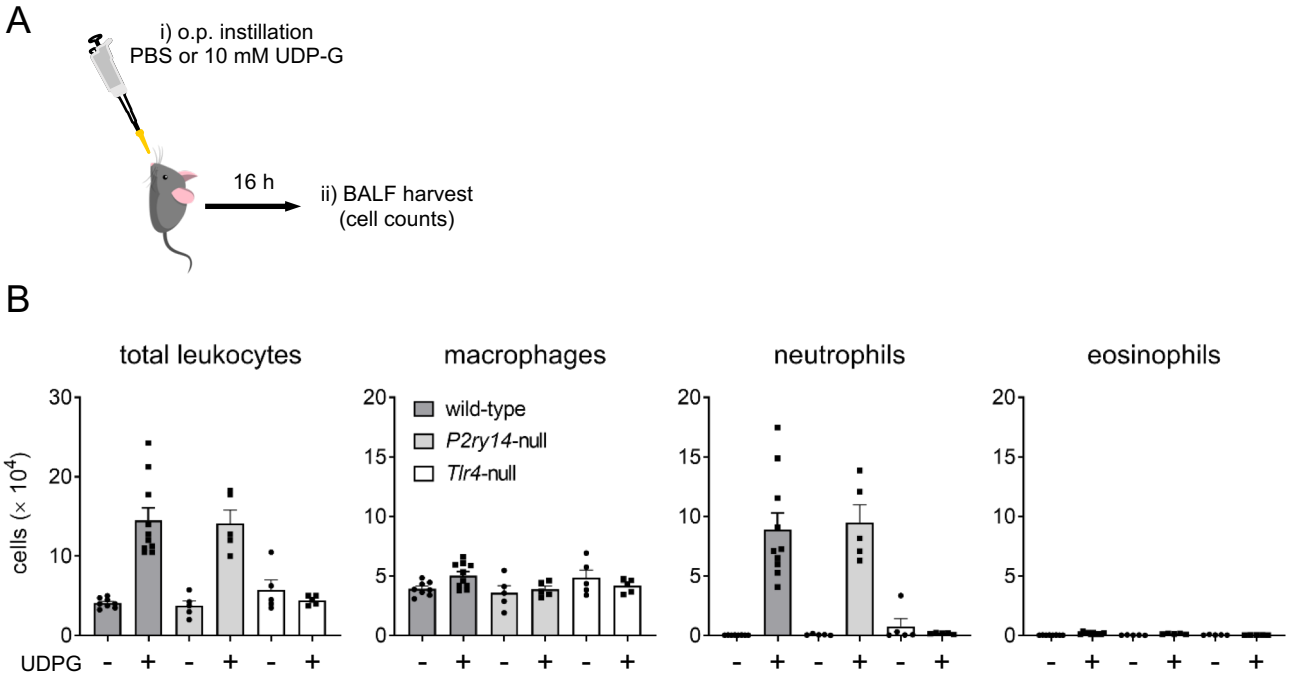

Supplemental Figure 2. Dependence of UDP-G-induced neutrophilic inflammation on TLR4, but not $P2Y_{14}R$. A) Schematic representation of the experiment. C57BL/6 wild-type, genetically-matched *P2ry14*$^{-/-}$ mice, or *Tlr4*$^{-/-}$ mice were given o.p. instillations of of 50 µl of 10 mM UDP-G in PBS (+), or PBS alone (-). **B**) Cell numbers for the indicated leukocyte populations in BALF at 16 h post-UDP-G instillation.

Supplemental Figure 3

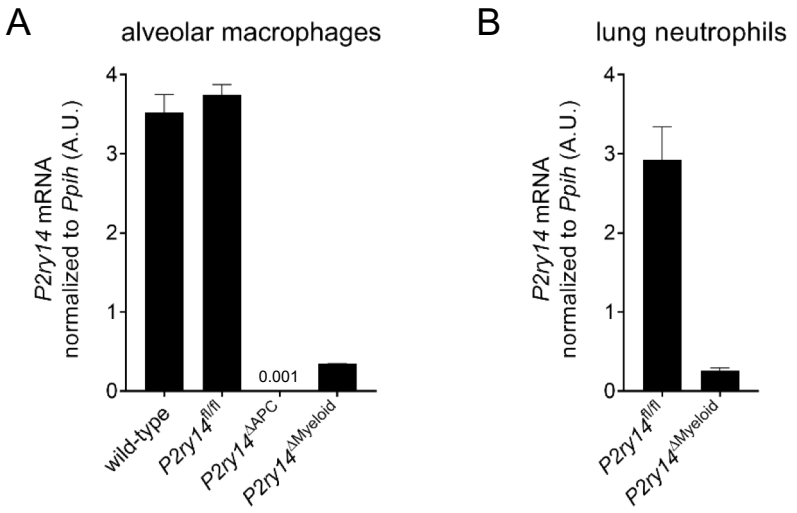

Supplemental Figure 3. Confirmation of *P2ry14* targeted deletion. A) Real-time PCR analysis of *P2ry14* transcripts in alveolar macrophages sorted from wild-type, *P2ry14*$^{fl/fl}$, *P2ry14*$^{\Delta APC}$ and *P2ry14*$^{\Delta Myeloid}$ mice. **B)** Detection of *P2ry14* mRNA in neutrophils sorted from lungs of *P2ry14*$^{fl/fl}$ and *P2ry14*$^{\Delta Myeloid}$ mice 16 h after *o.p.* administration of KC (0.35 µg) and LIX (0.35 µg).

Supplemental Figure 4

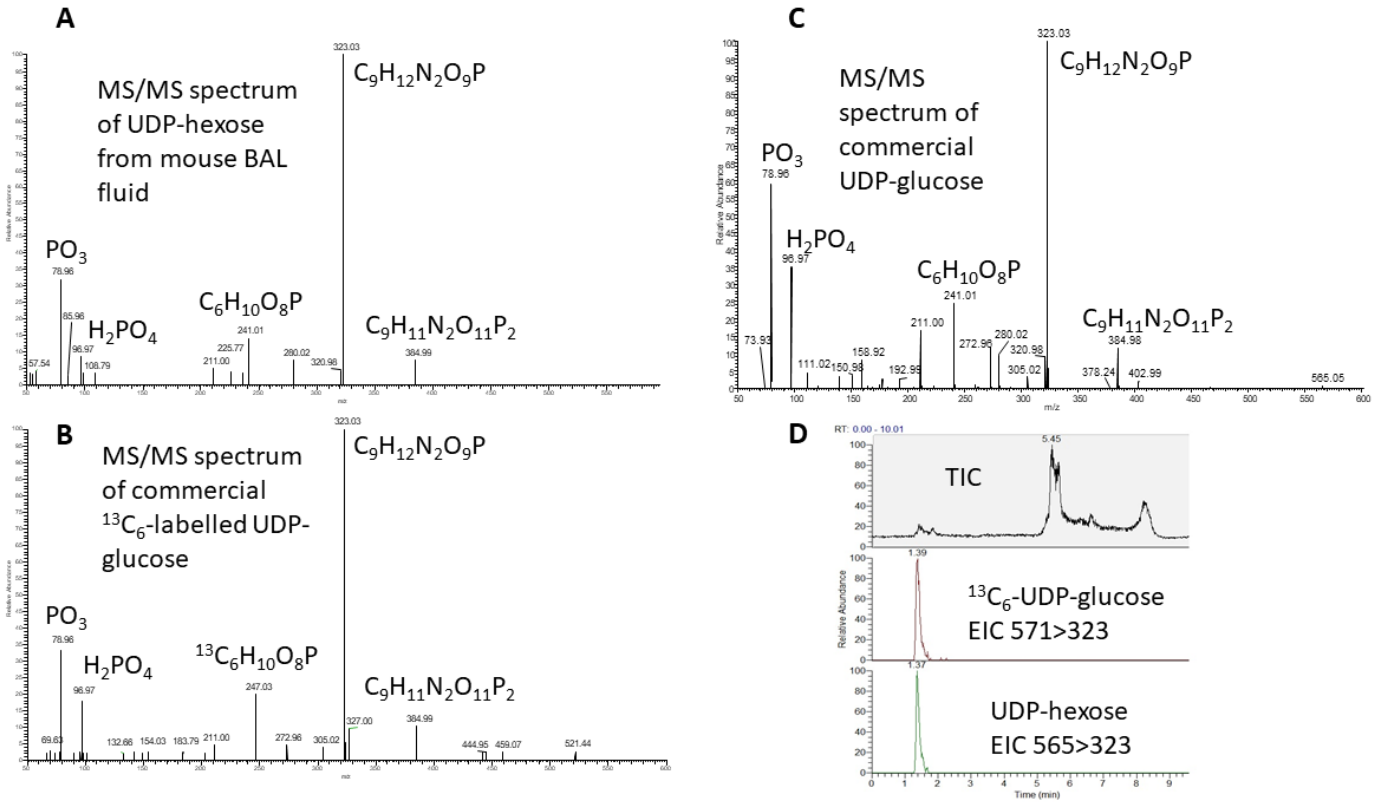

Supplemental Figure 4. Analysis of UDP-G in BALF. Comparison of the MSMS spectra of endogenous UDP-hexose **(A)** and of exogenously added ^{13}C-isotopically-labeled UDP-G **(B)** from mouse lavage fluid, and a commercially available (natural abundance) UDP-G **(C)** shows extensive overlap and confirm the identity of the m/z 565 ion as UDP-hexose. Of note, the ions in the MSMS fragmentation spectrum of the ^{13}C-isotopically-labeled UDP-G that correspond to glucose-containing fragments are appropriately mass shifted while fragments that do not contain the glucose moiety are not mass shifted. The total ion chromatogram (TIC) from mouse lavage fluid and the extracted ion chromatograms (EIC)s for the spiked-in, isotopically labeled UDP-G (571>323) and the endogenous UDP-hexose (565>323) are shown in panel **(D)**.

Supplemental Figure 5

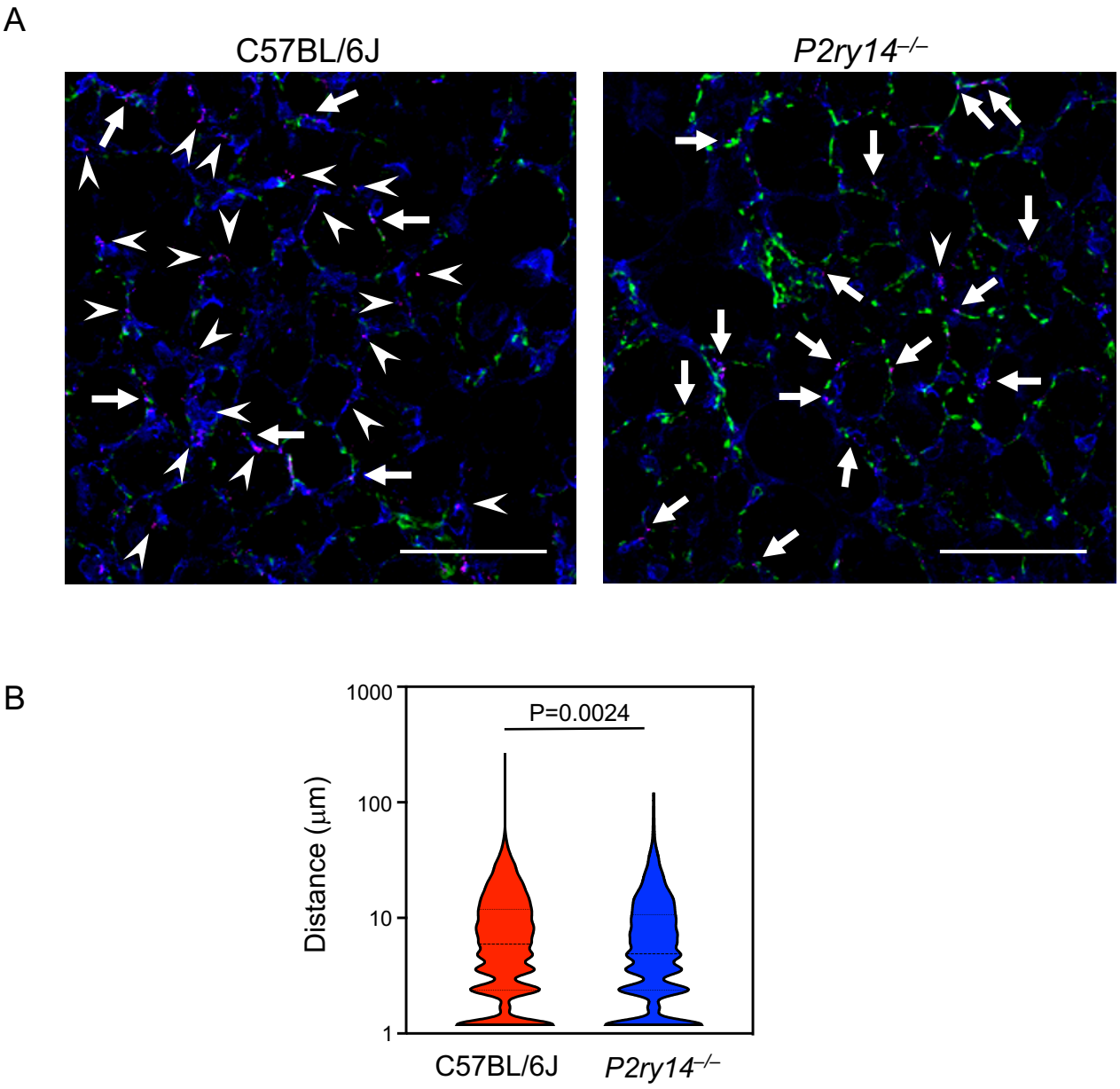

Supplemental Figure 5. Preferential association of *P2ry14* null eosinophils with endothelium. **A**) Images of precision cut lung slices (PCLS) stained for CCR3$^+$ eosinophils (magenta), CD31$^+$ endothelial cells (green) and CD324$^+$ epithelial cells (blue) 48 h after OVA challenge of ASP/OVA-sensitized mice. Arrows denote eosinophils associated with endothelial cells, whereas arrowheads denote eosinophils not associated with endothelial cells. **B**) Violin plots showing cumulative data for distances between eosinophils and the nearest epithelial cells in C57BL/6J (red) and *P2ry14*$^{-/-}$ mice (blue). Data were analyzed by unpaired two-tailed t-test (*n*=5000). White bar denotes 100 µm.

Supplemental Figure 6

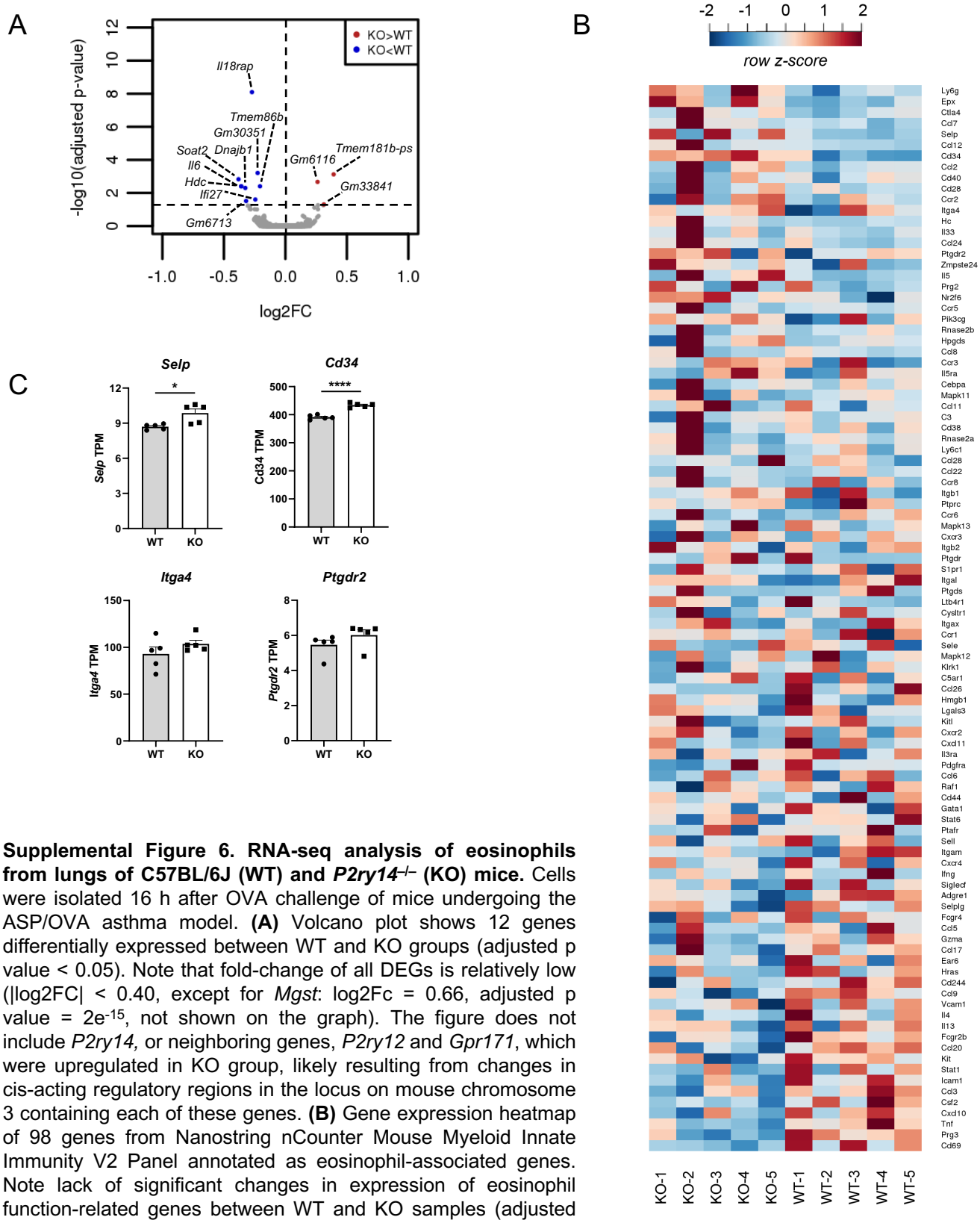

Supplemental Figure 6. RNA-seq analysis of eosinophils from lungs of C57BL/6J (WT) and *P2ry14*$^{-/-}$ (KO) mice. Cells were isolated 16 h after OVA challenge of mice undergoing the ASP/OVA asthma model. **(A)** Volcano plot shows 12 genes differentially expressed between WT and KO groups (adjusted p value < 0.05). Note that fold-change of all DEGs is relatively low (|log2FC| < 0.40, except for *Mgst*: log2Fc = 0.66, adjusted p value = 2e^{-15}, not shown on the graph). The figure does not include *P2ry14,* or neighboring genes, *P2ry12* and *Gpr171*, which were upregulated in KO group, likely resulting from changes in cis-acting regulatory regions in the locus on mouse chromosome 3 containing each of these genes. **(B)** Gene expression heatmap of 98 genes from Nanostring nCounter Mouse Myeloid Innate Immunity V2 Panel annotated as eosinophil-associated genes. Note lack of significant changes in expression of eosinophil function-related genes between WT and KO samples (adjusted p-value > 0.05). **(C)** Minor genotype-specific differences in expression of genes affecting adhesion.

Supplemental Figure 7

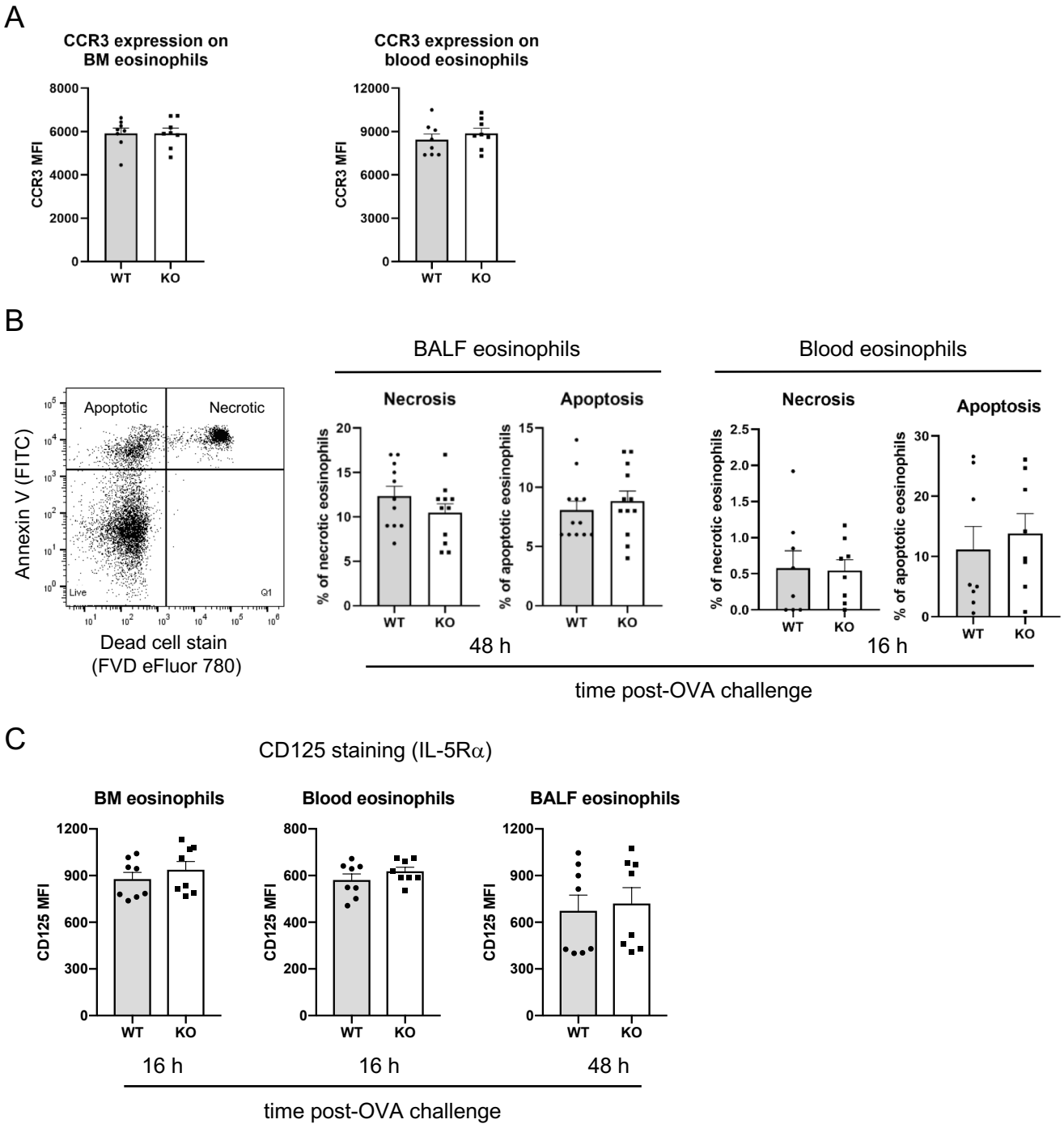

Supplemental Figure 7. Characteristics of *P2ry14* null eosinophils. **A**) CCR3 staining of wild type (WT) and *P2ry14*-deficient (KO) eosinophils from BM and blood. **B**) Flow cytometric staining for apoptotic (Annexin positive) and necrotic (dead cell stain positive) cells. **C)** Staining of eosinophils for CD125 (IL-5Rα).

Supplemental Figure 8

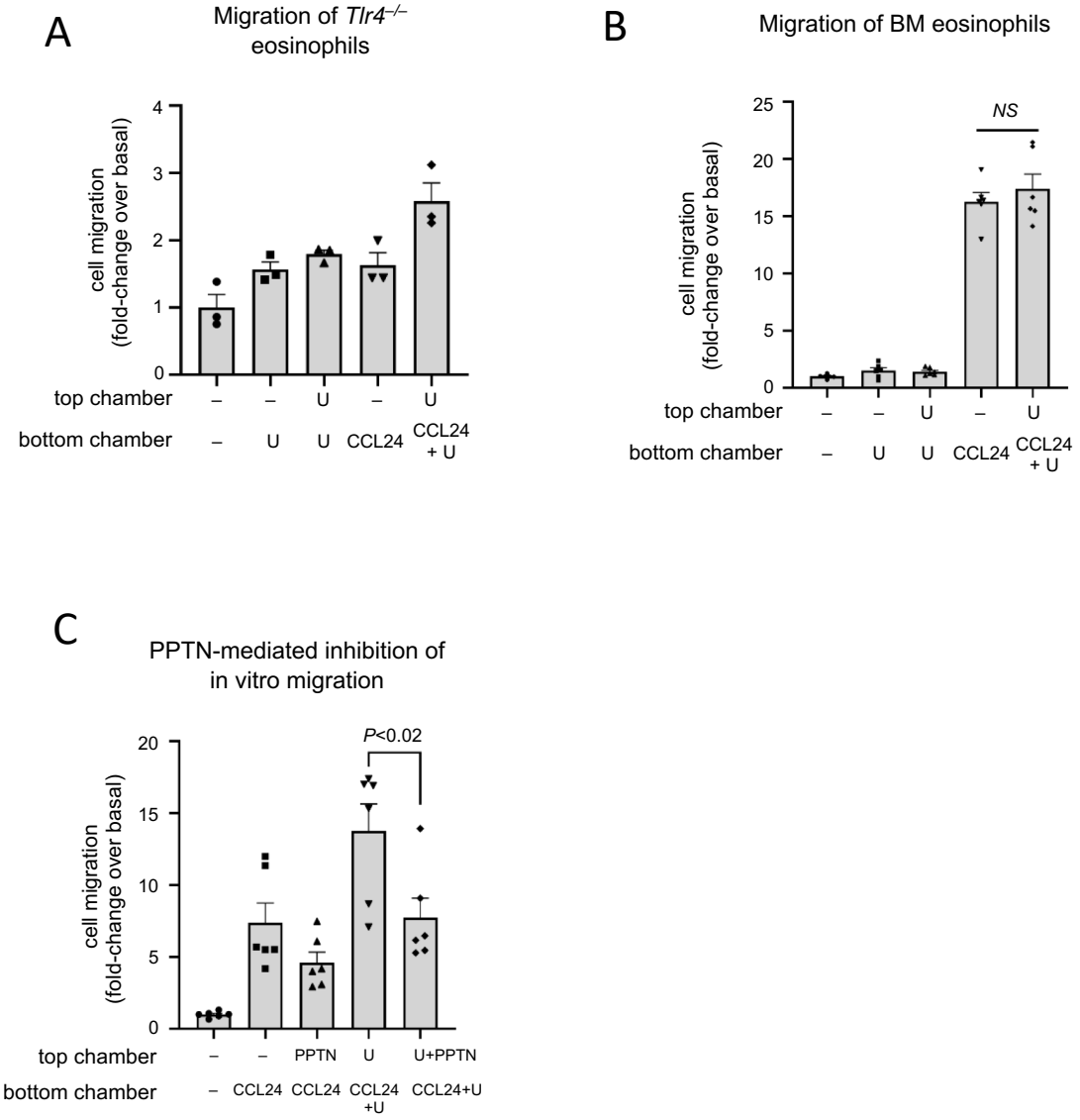

Supplemental Figure 8. *In vitro* migration of eosinophils. A) Migration of *Tlr4*$^{-/-}$ eosinophils in response to the indicated agents added to the top and/or bottom chambers of Transwell system plate. **B**) *In vitro* migration of BM eosinophils in response to UDP-glucose and CCL24. **C**) Inhibitory effect of PPTN on UDP-glucose-enhanced, CCL24-dependent migration of eosinophils. U, UDP-glucose

Supplemental Figure 9

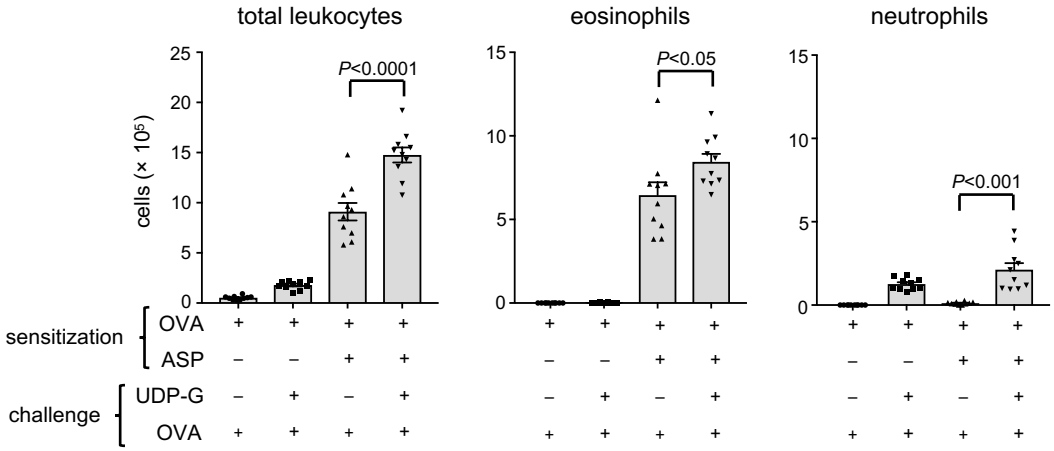

Supplemental Figure 9. Additive effect of exogenous UDP-G on OVA-induced eosinophil recruitment. Note that UDP-G-mediated neutrophil recruitment is endotoxin-dependent (see Supplemental Figure 1).

Supplemental Figure 10

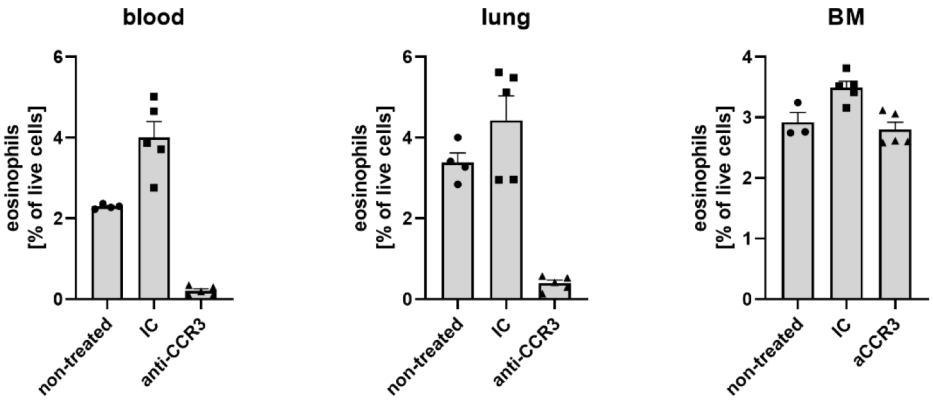

Supplemental Figure 10. Antibody-mediated depletion of eosinophils. Percentages of eosinophils in blood, lungs, and bone marrow of naïve mice receiving anti-CCR3 Ab or IC for 3 days and harvested on day 4.

Supplemental Figure 11

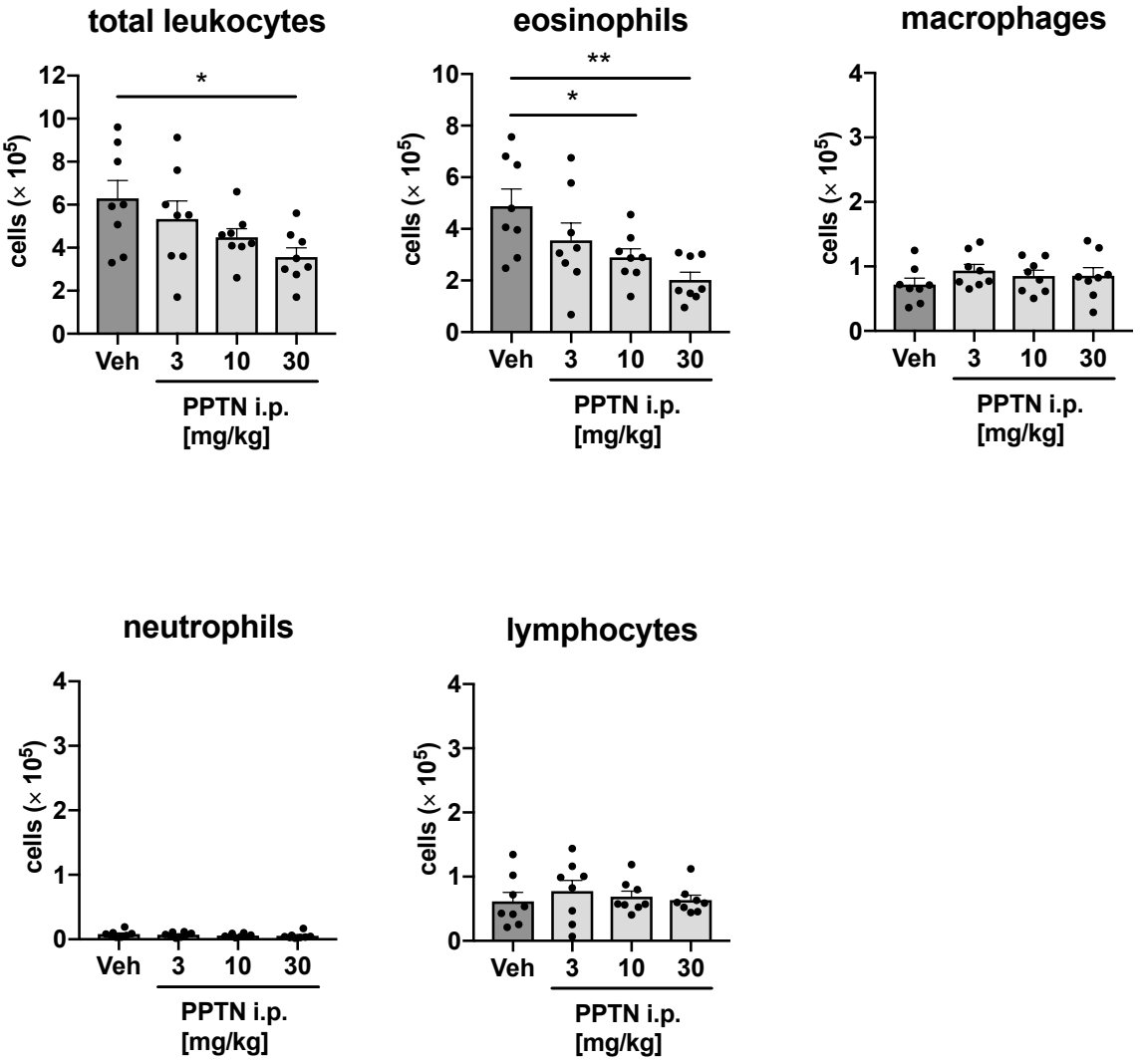

Supplemental Figure 11. Dose response of *in vivo* administration of PPTN. Shown are numbers of the indicated cell types recruited to the airways of mice sensitized with ASP/OVA, given the indicated doses of PPTN, and challenged with OVA.